

Search for the Standard Model Higgs Boson Produced in Association with a Z boson in $p\bar{p}$ Collisions at $\sqrt{s} = 1.96$ TeV

T. Aaltonen,²¹ B. Álvarez González^{y,9} S. Amerio,⁴⁰ D. Amidei,³² A. Anastassov^{w,15} A. Annovi,¹⁷ J. Antos,¹²
 G. Apollinari,¹⁵ J.A. Appel,¹⁵ T. Arisawa,⁵⁴ A. Artikov,¹³ J. Asaadi,⁴⁹ W. Ashmanskas,¹⁵ B. Auerbach,⁵⁷
 A. Aurisano,⁴⁹ F. Azfar,³⁹ W. Badgett,¹⁵ T. Bae,²⁵ A. Barbaro-Galtieri,²⁶ V.E. Barnes,⁴⁴ B.A. Barnett,²³
 P. Barria^{gg,42} P. Bartos,¹² M. Bauc^{ee,40} F. Bedeschi,⁴² S. Behari,²³ G. Bellettini^{ff,42} J. Bellinger,⁵⁶ D. Benjamin,¹⁴
 A. Beretvas,¹⁵ A. Bhatti,⁴⁶ D. Bisello^{ee,40} I. Bizjak,²⁸ K.R. Bland,⁵ B. Blumenfeld,²³ A. Bocci,¹⁴ A. Bodek,⁴⁵
 D. Bortoletto,⁴⁴ J. Boudreau,⁴³ A. Boveia,¹¹ L. Brigliadori^{dd,6} C. Bromberg,³³ E. Brucken,²¹ J. Budagov,¹³
 H.S. Budd,⁴⁵ K. Burkett,¹⁵ G. Busetto^{ee,40} P. Bussey,¹⁹ A. Buzatu,³¹ A. Calamba,¹⁰ C. Calancha,²⁹ S. Camarda,⁴
 M. Campanelli,²⁸ M. Campbell,³² F. Canelli^{11,15} B. Carls,²² D. Carlsmith,⁵⁶ R. Carosi,⁵⁸ S. Carrillo^{l,16}
 S. Carron,¹⁵ B. Casal^{k,9} M. Casarsa,⁵⁰ A. Castro^{dd,6} P. Catastini,²⁰ D. Cauz,⁵⁰ V. Cavaliere,²² M. Cavalli-Sforza,⁴
 A. Cerri^{f,26} L. Cerrito^{r,28} Y.C. Chen,¹ M. Chertok,⁷ G. Chiarelli,⁵⁸ G. Chlachidze,¹⁵ F. Chlebana,¹⁵ K. Cho,²⁵
 D. Chokheli,¹³ W.H. Chung,⁵⁶ Y.S. Chung,⁴⁵ M.A. Ciocci^{gg,42} A. Clark,¹⁸ C. Clarke,⁵⁵ G. Compostella^{ee,40}
 M.E. Convery,¹⁵ J. Conway,⁷ M. Corbo,¹⁵ M. Cordelli,¹⁷ C.A. Cox,⁷ D.J. Cox,⁷ F. Crescioli^{ff,42} J. Cuevas^{y,9}
 R. Culbertson,¹⁵ D. Dagenhart,¹⁵ N. d'Ascenzo^{v,15} M. Datta,¹⁵ P. de Barbaro,⁴⁵ M. Dell'Orso^{ff,42} L. Demortier,⁴⁶
 M. Deninno,⁶ F. Devoto,²¹ M. d'Errico^{ee,40} A. Di Canto^{ff,42} B. Di Ruzza,¹⁵ J.R. Dittmann,⁵ M. D'Onofrio,²⁷
 S. Donati^{ff,42} P. Dong,¹⁵ M. Dorigo,⁵⁰ T. Dorigo,⁴⁰ K. Ebina,⁵⁴ A. Elagin,⁴⁹ A. Eppig,³² R. Erbacher,⁷ S. Errede,²²
 N. Ershaidat^{cc,15} R. Eusebi,⁴⁹ S. Farrington,³⁹ M. Feindt,²⁴ J.P. Fernandez,²⁹ R. Field,¹⁶ G. Flanagan^{t,15}
 R. Forrest,⁷ M.J. Frank,⁵ M. Franklin,²⁰ J.C. Freeman,¹⁵ Y. Funakoshi,⁵⁴ I. Furic,¹⁶ M. Gallinaro,⁴⁶ J.E. Garcia,¹⁸
 A.F. Garfinkel,⁴⁴ P. Garosi^{gg,42} H. Gerberich,²² E. Gerchtein,¹⁵ S. Giagu,⁴⁷ V. Giakoumopoulou,³ P. Giannetti,⁴²
 K. Gibson,⁴³ C.M. Ginsburg,¹⁵ N. Giokaris,³ P. Giromini,¹⁷ G. Giurgiu,²³ V. Glagolev,¹³ D. Glenzinski,¹⁵
 M. Gold,³⁵ D. Goldin,⁴⁹ N. Goldschmidt,¹⁶ A. Golossanov,¹⁵ G. Gomez,⁹ G. Gomez-Ceballos,³⁰ M. Goncharov,³⁰
 O. González,²⁹ I. Gorelov,³⁵ A.T. Goshaw,¹⁴ K. Goulianos,⁴⁶ S. Grinstein,⁴ C. Grosso-Pilcher,¹¹ R.C. Group^{53,15}
 J. Guimaraes da Costa,²⁰ S.R. Hahn,¹⁵ E. Halkiadakis,⁴⁸ A. Hamaguchi,³⁸ J.Y. Han,⁴⁵ F. Happacher,¹⁷ K. Hara,⁵¹
 D. Hare,⁴⁸ M. Hare,⁵² R.F. Harr,⁵⁵ K. Hatakeyama,⁵ C. Hays,³⁹ M. Heck,²⁴ J. Heinrich,⁴¹ M. Herndon,⁵⁶
 S. Hewamanage,⁵ A. Hocker,¹⁵ W. Hopkins^{g,15} D. Horn,²⁴ S. Hou,¹ R.E. Hughes,³⁶ M. Hurwitz,¹¹ U. Husemann,⁵⁷
 N. Hussain,³¹ M. Hussein,³³ J. Huston,³³ G. Introzzi,⁴² M. Iori^{hh,47} A. Ivanov^{p,7} E. James,¹⁵ D. Jang,¹⁰
 B. Jayatilaka,¹⁴ E.J. Jeon,²⁵ S. Jindariani,¹⁵ M. Jones,⁴⁴ K.K. Joo,²⁵ S.Y. Jun,¹⁰ T.R. Junk,¹⁵ T. Kamon^{25,49}
 P.E. Karchin,⁵⁵ A. Kasmi,⁵ Y. Kato^{o,38} W. Ketchum,¹¹ J. Keung,⁴¹ V. Khotilovich,⁴⁹ B. Kilminster,¹⁵ D.H. Kim,²⁵
 H.S. Kim,²⁵ J.E. Kim,²⁵ M.J. Kim,¹⁷ S.B. Kim,²⁵ S.H. Kim,⁵¹ Y.K. Kim,¹¹ Y.J. Kim,²⁵ N. Kimura,⁵⁴ M. Kirby,¹⁵
 S. Klimentenko,¹⁶ K. Knoepfel,¹⁵ K. Kondo^{*,54} D.J. Kong,²⁵ J. Konigsberg,¹⁶ A.V. Kotwal,¹⁴ M. Kreps,²⁴ J. Kroll,⁴¹
 D. Krop,¹¹ M. Kruse,¹⁴ V. Krutelyov^{c,49} T. Kuhr,²⁴ M. Kurata,⁵¹ S. Kwang,¹¹ A.T. Laasanen,⁴⁴ S. Lami,⁴²
 S. Lammel,¹⁵ M. Lancaster,²⁸ R.L. Lander,⁷ K. Lannon^{x,36} A. Lath,⁴⁸ G. Latino^{ff,42} T. LeCompte,² E. Lee,⁴⁹
 H.S. Lee^{25,11} J.S. Lee,²⁵ S.W. Lee^{aa,49} S. Leo^{ff,42} S. Leone,⁴² J.D. Lewis,¹⁵ A. Limosani^{s,14} C.-J. Lin,²⁶
 M. Lindgren,¹⁵ E. Lipeles,⁴¹ A. Lister,¹⁸ D.O. Litvintsev,¹⁵ C. Liu,⁴³ H. Liu,⁵³ Q. Liu,⁴⁴ T. Liu,¹⁵ S. Lockwitz,⁵⁷
 A. Loginov,⁵⁷ D. Lucchesi^{ee,40} J. Lueck,²⁴ P. Lujan,²⁶ P. Lukens,¹⁵ G. Lungu,⁴⁶ J. Lys,²⁶ R. Lysak^{e,12} R. Madrak,¹⁵
 K. Maeshima,¹⁵ P. Maestro^{gg,42} S. Malik,⁴⁶ G. Manca^{a,27} A. Manousakis-Katsikakis,³ F. Margaroli,⁴⁷ C. Marino,²⁴
 M. Martínez,⁴ P. Mastrandrea,⁴⁷ K. Matera,²² M.E. Mattson,⁵⁵ A. Mazzacane,¹⁵ P. Mazzanti,⁵⁹ K.S. McFarland,⁴⁵
 P. McIntyre,⁴⁹ R. McNulty^{j,27} A. Mehta,²⁷ P. Mehtala,²¹ C. Mesropian,⁴⁶ T. Miao,¹⁵ D. Mietlicki,³² A. Mitra,¹
 H. Miyake,⁵¹ S. Moed,¹⁵ N. Moggi,⁶ M.N. Mondragon^{m,15} C.S. Moon,²⁵ R. Moore,¹⁵ M.J. Morello^{hh,42} J. Morlock,²⁴
 P. Movilla Fernandez,¹⁵ A. Mukherjee,¹⁵ Th. Muller,²⁴ P. Murat,¹⁵ M. Mussini^{dd,6} J. Nachtman^{n,15} Y. Nagai,⁵¹
 J. Naganoma,⁵⁴ I. Nakano,³⁷ A. Napier,⁵² J. Nett,⁴⁹ C. Neu,⁵³ M.S. Neubauer,²² J. Nielsen^{d,26} L. Nodulman,²
 S.Y. Noh,²⁵ O. Norriella,²² L. Oakes,³⁹ S.H. Oh,¹⁴ Y.D. Oh,²⁵ I. Oksuzian,⁵³ T. Okusawa,³⁸ R. Orava,²¹
 L. Ortolan,⁴ S. Pagan Griso^{ee,40} C. Pagliarone,⁵⁰ E. Palencia^{f,9} V. Papadimitriou,¹⁵ A.A. Paramonov,² J. Patrick,¹⁵
 G. Pauletta^{jj,50} M. Paulini,¹⁰ C. Paus,³⁰ D.E. Pellett,⁷ A. Penzo,⁶⁰ T.J. Phillips,¹⁴ G. Piacentino,⁴² E. Pianori,⁴¹
 J. Pilot,³⁶ K. Pitts,²² C. Plager,⁸ L. Pondrom,⁵⁶ S. Poprocki^{g,15} K. Potamianos,⁴⁴ F. Prokoshin^{bb,13} A. Pranko,²⁶
 F. Ptohos^{h,17} G. Punzi^{ff,42} A. Rahaman,⁴³ V. Ramakrishnan,⁵⁶ N. Ranjan,⁴⁴ I. Redondo,²⁹ P. Renton,³⁹
 M. Rescigno,⁶¹ T. Riddick,²⁸ F. Rimondi^{dd,6} L. Ristori,^{42,15} A. Robson,¹⁹ T. Rodrigo,⁹ T. Rodriguez,⁴¹ E. Rogers,²²
 S. Rolli^{i,52} R. Roser,¹⁵ F. Ruffini^{gg,42} A. Ruiz,⁹ J. Russ,¹⁰ V. Rusu,¹⁵ A. Safonov,⁴⁹ W.K. Sakumoto,⁴⁵ Y. Sakurai,⁵⁴
 L. Santi^{jj,50} K. Sato,⁵¹ V. Saveliev^{v,15} A. Savoy-Navarro^{z,15} P. Schlabach,¹⁵ A. Schmidt,²⁴ E.E. Schmidt,¹⁵

T. Schwarz,¹⁵ L. Scodellaro,⁹ A. Scribano^{gg, 42} F. Scuri,⁴² S. Seidel,³⁵ Y. Seiya,³⁸ A. Semenov,¹³ F. Sforza^{gg, 42} S.Z. Shalhout,⁷ T. Shears,²⁷ P.F. Shepard,⁴³ M. Shimojima^{u, 51} M. Shochet,¹¹ I. Shreyber-Tecker,³⁴ A. Simonenko,¹³ P. Sinervo,³¹ K. Sliwa,⁵² J.R. Smith,⁷ F.D. Snider,¹⁵ A. Soha,¹⁵ V. Sorin,⁴ H. Song,⁴³ P. Squillacioti^{gg, 42} M. Stancari,¹⁵ R. St. Denis,¹⁹ B. Stelzer,³¹ O. Stelzer-Chilton,³¹ D. Stentz^{w, 15} J. Strologas,³⁵ G.L. Strycker,³² Y. Sudo,⁵¹ A. Sukhanov,¹⁵ I. Suslov,¹³ K. Takemasa,⁵¹ Y. Takeuchi,⁵¹ J. Tang,¹¹ M. Tecchio,³² P.K. Teng,¹ J. Thom^{g, 15} J. Thome,¹⁰ G.A. Thompson,²² E. Thomson,⁴¹ P. Tipton,⁵⁷ D. Toback,⁴⁹ S. Tokar,¹² K. Tollefson,³³ T. Tomura,⁵¹ D. Tonelli,¹⁵ S. Torre,¹⁷ D. Torretta,¹⁵ P. Totaro,⁴⁰ M. Trovato^{hh, 42} F. Ukegawa,⁵¹ S. Uozumi,²⁵ A. Varganov,³² F. Vázquez^{m, 16} G. Velev,¹⁵ C. Vellidis,¹⁵ M. Vidal,⁴⁴ I. Vila,⁹ R. Vilar,⁹ J. Vizán,⁹ M. Vogel,³⁵ G. Volpi,¹⁷ P. Wagner,⁴¹ R.L. Wagner,¹⁵ T. Wakisaka,³⁸ R. Wallny,⁸ S.M. Wang,¹ A. Warburton,³¹ D. Waters,²⁸ W.C. Wester III,¹⁵ D. Whiteson^{b, 41} A.B. Wicklund,² E. Wicklund,¹⁵ S. Wilbur,¹¹ F. Wick,²⁴ H.H. Williams,⁴¹ J.S. Wilson,³⁶ P. Wilson,¹⁵ B.L. Winer,³⁶ P. Wittich^{g, 15} S. Wolbers,¹⁵ H. Wolfe,³⁶ T. Wright,³² X. Wu,¹⁸ Z. Wu,⁵ K. Yamamoto,³⁸ D. Yamato,³⁸ T. Yang,¹⁵ U.K. Yang^{q, 11} Y.C. Yang,²⁵ W.-M. Yao,²⁶ G.P. Yeh,¹⁵ K. Yi^{n, 15} J. Yoh,¹⁵ K. Yorita,⁵⁴ T. Yoshida^{l, 38} G.B. Yu,¹⁴ I. Yu,²⁵ S.S. Yu,¹⁵ J.C. Yun,¹⁵ A. Zanetti,⁵⁰ Y. Zeng,¹⁴ and S. Zucchelli^{dd6}

(CDF Collaboration[†])

¹*Institute of Physics, Academia Sinica, Taipei, Taiwan 11529, Republic of China*

²*Argonne National Laboratory, Argonne, Illinois 60439, USA*

³*University of Athens, 157 71 Athens, Greece*

⁴*Institut de Física d'Altes Energies, ICREA, Universitat Autònoma de Barcelona, E-08193, Bellaterra (Barcelona), Spain*

⁵*Baylor University, Waco, Texas 76798, USA*

⁶*Istituto Nazionale di Fisica Nucleare Bologna, ^{dd}University of Bologna, I-40127 Bologna, Italy*

⁷*University of California, Davis, Davis, California 95616, USA*

⁸*University of California, Los Angeles, Los Angeles, California 90024, USA*

⁹*Instituto de Física de Cantabria, CSIC-University of Cantabria, 39005 Santander, Spain*

¹⁰*Carnegie Mellon University, Pittsburgh, Pennsylvania 15213, USA*

¹¹*Enrico Fermi Institute, University of Chicago, Chicago, Illinois 60637, USA*

¹²*Comenius University, 842 48 Bratislava, Slovakia; Institute of Experimental Physics, 040 01 Kosice, Slovakia*

¹³*Joint Institute for Nuclear Research, RU-141980 Dubna, Russia*

¹⁴*Duke University, Durham, North Carolina 27708, USA*

¹⁵*Fermi National Accelerator Laboratory, Batavia, Illinois 60510, USA*

¹⁶*University of Florida, Gainesville, Florida 32611, USA*

¹⁷*Laboratori Nazionali di Frascati, Istituto Nazionale di Fisica Nucleare, I-00044 Frascati, Italy*

¹⁸*University of Geneva, CH-1211 Geneva 4, Switzerland*

¹⁹*Glasgow University, Glasgow G12 8QQ, United Kingdom*

²⁰*Harvard University, Cambridge, Massachusetts 02138, USA*

²¹*Division of High Energy Physics, Department of Physics,*

University of Helsinki and Helsinki Institute of Physics, FIN-00014, Helsinki, Finland

²²*University of Illinois, Urbana, Illinois 61801, USA*

²³*The Johns Hopkins University, Baltimore, Maryland 21218, USA*

²⁴*Institut für Experimentelle Kernphysik, Karlsruhe Institute of Technology, D-76131 Karlsruhe, Germany*

²⁵*Center for High Energy Physics: Kyungpook National University,*

Daegu 702-701, Korea; Seoul National University, Seoul 151-742,

Korea; Sungkyunkwan University, Suwon 440-746,

Korea; Korea Institute of Science and Technology Information,

Daejeon 305-806, Korea; Chonnam National University, Gwangju 500-757,

Korea; Chonbuk National University, Jeonju 561-756, Korea

²⁶*Ernest Orlando Lawrence Berkeley National Laboratory, Berkeley, California 94720, USA*

²⁷*University of Liverpool, Liverpool L69 7ZE, United Kingdom*

²⁸*University College London, London WC1E 6BT, United Kingdom*

²⁹*Centro de Investigaciones Energéticas Medioambientales y Tecnológicas, E-28040 Madrid, Spain*

³⁰*Massachusetts Institute of Technology, Cambridge, Massachusetts 02139, USA*

³¹*Institute of Particle Physics: McGill University, Montréal, Québec,*

Canada H3A 2T8; Simon Fraser University, Burnaby, British Columbia,

Canada V5A 1S6; University of Toronto, Toronto, Ontario,

Canada M5S 1A7; and TRIUMF, Vancouver, British Columbia, Canada V6T 2A3

³²*University of Michigan, Ann Arbor, Michigan 48109, USA*

³³*Michigan State University, East Lansing, Michigan 48824, USA*

³⁴*Institution for Theoretical and Experimental Physics, ITEP, Moscow 117259, Russia*

³⁵*University of New Mexico, Albuquerque, New Mexico 87131, USA*

³⁶*The Ohio State University, Columbus, Ohio 43210, USA*

³⁷*Okayama University, Okayama 700-8530, Japan*

- ³⁸Osaka City University, Osaka 588, Japan
³⁹University of Oxford, Oxford OX1 3RH, United Kingdom
⁴⁰Istituto Nazionale di Fisica Nucleare, Sezione di Padova-Trento, ^{ee}University of Padova, I-35131 Padova, Italy
⁴¹University of Pennsylvania, Philadelphia, Pennsylvania 19104, USA
⁴²Istituto Nazionale di Fisica Nucleare Pisa, ^{ff}University of Pisa,
^{gg}University of Siena and ^{hh}Scuola Normale Superiore, I-56127 Pisa, Italy
⁴³University of Pittsburgh, Pittsburgh, Pennsylvania 15260, USA
⁴⁴Purdue University, West Lafayette, Indiana 47907, USA
⁴⁵University of Rochester, Rochester, New York 14627, USA
⁴⁶The Rockefeller University, New York, New York 10065, USA
⁴⁷Istituto Nazionale di Fisica Nucleare, Sezione di Roma 1,
ⁱⁱSapienza Università di Roma, I-00185 Roma, Italy
⁴⁸Rutgers University, Piscataway, New Jersey 08855, USA
⁴⁹Texas A&M University, College Station, Texas 77843, USA
⁵⁰Istituto Nazionale di Fisica Nucleare Trieste/Udine,
I-34100 Trieste, ^{jj}University of Udine, I-33100 Udine, Italy
⁵¹University of Tsukuba, Tsukuba, Ibaraki 305, Japan
⁵²Tufts University, Medford, Massachusetts 02155, USA
⁵³University of Virginia, Charlottesville, Virginia 22906, USA
⁵⁴Waseda University, Tokyo 169, Japan
⁵⁵Wayne State University, Detroit, Michigan 48201, USA
⁵⁶University of Wisconsin, Madison, Wisconsin 53706, USA
⁵⁷Yale University, New Haven, Connecticut 06520, USA
⁵⁸Istituto Nazionale di Fisica Nucleare Pisa, ^{ff}University of Pisa,
^{ff}University of Siena and ^{gg}Scuola Normale Superiore, I-56127 Pisa, Italy
⁵⁹Istituto Nazionale di Fisica Nucleare Bologna, University of Bologna, I-40127 Bologna, Italy
⁶⁰Istituto Nazionale di Fisica Nucleare Trieste/Udine,
I-34100 Trieste, ⁱⁱUniversity of Udine, I-33100 Udine, Italy
⁶¹Istituto Nazionale di Fisica Nucleare, Sezione di Roma 1,
^{hh}Sapienza Università di Roma, I-00185 Roma, Italy
(Dated: March 21, 2012)

We present a search for the standard model Higgs boson produced in association with a Z boson, using up to 7.9 fb^{-1} of integrated luminosity from $p\bar{p}$ collisions collected with the CDF II detector. We utilize several novel techniques, including multivariate lepton selection, multivariate trigger parametrization, and a multi-stage signal discriminant consisting of specialized functions trained to distinguish individual backgrounds. By increasing acceptance and enhancing signal discrimination, these techniques have significantly improved the sensitivity of the analysis above what was expected from a larger dataset alone. We observe no significant evidence for a signal, and we set limits on the ZH production cross section. For a Higgs boson with mass $115 \text{ GeV}/c^2$, we expect (observe) a limit of 3.9 (4.8) times the standard model predicted value, at the 95% credibility level.

PACS numbers: 14.80.Bn, 13.85.Rm

*Deceased

†With visitors from ^aIstituto Nazionale di Fisica Nucleare, Sezione di Cagliari, 09042 Monserrato (Cagliari), Italy, ^bUniversity of CA Irvine, Irvine, CA 92697, USA, ^cUniversity of CA Santa Barbara, Santa Barbara, CA 93106, USA, ^dUniversity of CA Santa Cruz, Santa Cruz, CA 95064, USA, ^eInstitute of Physics, Academy of Sciences of the Czech Republic, Czech Republic, ^fCERN, CH-1211 Geneva, Switzerland, ^gCornell University, Ithaca, NY 14853, USA, ^hUniversity of Cyprus, Nicosia CY-1678, Cyprus, ⁱOffice of Science, U.S. Department of Energy, Washington, DC 20585, USA, ^jUniversity College Dublin, Dublin 4, Ireland, ^kETH, 8092 Zurich, Switzerland, ^lUniversity of Fukui, Fukui City, Fukui Prefecture, Japan 910-0017, ^mUniversidad Iberoamericana, Mexico D.F., Mexico, ⁿUniversity of Iowa, Iowa City, IA 52242, USA, ^oKinki University, Higashi-Osaka City, Japan 577-8502, ^pKansas State University, Manhattan, KS 66506, USA, ^qUniversity of Manchester, Manchester M13 9PL, United Kingdom, ^rQueen Mary, Univer-

The Higgs boson is the remaining unobserved particle of the standard model (SM) [1–3] predicted by the Higgs mechanism, which is postulated to describe the origin of electroweak symmetry breaking and elementary particle masses. Direct searches at LEP and the Tevatron have excluded SM Higgs bosons with masses (m_H) below 114.4

sity of London, London, E1 4NS, United Kingdom, ^sUniversity of Melbourne, Victoria 3010, Australia, ^tMuons, Inc., Batavia, IL 60510, USA, ^uNagasaki Institute of Applied Science, Nagasaki, Japan, ^vNational Research Nuclear University, Moscow, Russia, ^wNorthwestern University, Evanston, IL 60208, USA, ^xUniversity of Notre Dame, Notre Dame, IN 46556, USA, ^yUniversidad de Oviedo, E-33007 Oviedo, Spain, ^zCNRS-IN2P3, Paris, F-75252 France, ^{aa}Texas Tech University, Lubbock, TX 79609, USA, ^{bb}Universidad Tecnica Federico Santa Maria, 110v Valparaiso, Chile, ^{cc}Yarmouk University, Irbid 211-63, Jordan,

GeV/ c^2 [4] and in the range $156 \leq m_H \leq 177$ GeV/ c^2 [5], respectively, at the 95% credibility level (CL). Recent results from the ATLAS and CMS experiments [6, 7] have extended the excluded range of masses to $127 \leq m_H \leq 600$ GeV/ c^2 (at the 95% confidence level).

Production of Higgs bosons at the Tevatron primarily proceeds through the gluon fusion mechanism, $gg \rightarrow H$ [8]. Low-mass Higgs bosons ($m_H < 135$ GeV/ c^2) decay predominantly to a pair of b quarks, with a branching fraction of 79% (40%) [8] for $m_H = 100$ (135) GeV/ c^2 . Due to overwhelming QCD multijet production, low-mass searches with Higgs production via gluon fusion and $H \rightarrow b\bar{b}$ decay are not feasible. To overcome this difficulty, we utilize the associated production of a Higgs boson with a massive vector boson, where leptonic decays of the vector boson produce distinctive event signatures.

This Letter presents a search for the SM Higgs boson using the $ZH \rightarrow \ell^+\ell^-b\bar{b}$ process, where ℓ is an electron (e) or muon (μ). We search for events containing two oppositely-charged leptons consistent with the decay of a Z boson, and a hadronic signature consistent with the $H \rightarrow b\bar{b}$ decay mode. Previous searches [9, 10] by the CDF and D0 collaborations have demonstrated that this final state provides good sensitivity to a Higgs boson signal, primarily due to the ability of the experiments to reconstruct both the Z and Higgs bosons. We study data from $p\bar{p}$ collisions at $\sqrt{s} = 1.96$ TeV recorded by the CDF II detector. We combine two independent analyses, one with $Z \rightarrow e^+e^-$ [11] and one with $Z \rightarrow \mu^+\mu^-$ [12], using data corresponding to 7.5 and 7.9 fb $^{-1}$ of integrated luminosity, respectively.

The CDF II detector [13] consists of silicon-based and wire-drift-chamber tracking systems immersed in a 1.4 T magnetic field for particle momentum determination. Surrounding the tracking systems are electromagnetic and hadronic calorimeters, providing coverage in the pseudorapidity [14] range $|\eta| < 3.6$. Additional drift chambers used for muon identification are located in the outermost layer of the detector.

The sensitivity of this updated analysis is enhanced by using several novel techniques following two general strategies: increasing acceptance and enhancing signal discrimination. To increase acceptance, we introduce artificial neural networks (NNs) for lepton selection, and we also use several online event-selection (trigger) algorithms not previously used. Using a new technique, we are able to accurately model the combined behavior of these triggers, allowing access to ZH candidate events beyond the reach of the previous CDF searches. To enhance signal discrimination, we form a multi-stage event discriminant organized to isolate ZH candidates from known SM and instrumental processes (backgrounds).

To improve on standard cut-based lepton identification, we instead select leptons consistent with the decay of a Z boson by using several NNs. Each NN identifies individual electrons or muons, distinguishing them from

both non-leptonic candidates and true leptons not originating from Z decays. A single NN is used for muon identification, and is trained [15] to distinguish between true muons from simulated Z decays and misidentified muons from a data sample containing same-charge muon candidates. In events with $Z \rightarrow \mu\mu$ decays well contained in the detector, the muon NN selection achieves a Z identification efficiency of $\sim 96\%$, while simultaneously rejecting $\sim 94\%$ of the non- Z background. Detector geometry [16, 17] motivates three NNs for electron identification. One is optimized for identification in the pseudorapidity range $|\eta| < 1.1$. The other two NNs are trained for the forward regions; one considers only candidates with a silicon-based track and the other considers candidates without such a track in the region $1.1 \leq |\eta| \leq 2.8$. Compared to the selection utilized in previous searches, the electron NN has improved the rejection of jets misidentified as electrons by a factor of five. In total, the multivariate lepton selection has increased the acceptance of the analysis by $\sim 20\%$ over previous searches [9].

Complementary to the improved lepton identification, we add additional triggers that were not previously utilized in this analysis channel. Rather than using a single trigger with a threshold for muon p_T or electron E_T for the respective Z selection, we consider any event selected by any trigger in three general sets. The first set includes several triggers that select events containing muon detector and drift chamber activity indicative of a high- p_T muon [18, 19]. Included in this category may be triggers with lower p_T thresholds than the default muon trigger. The second set of triggers selects events with a large calorimeter-energy imbalance (missing transverse energy, \cancel{E}_T [20]). Some of these events contain muons that are not selected with the high- p_T muon trigger, thereby increasing the acceptance of this analysis. A third set of triggers selects events with activity in the calorimeter suggestive of a high- E_T electron [21]. By using these sets of triggers rather than just single triggers for each lepton type, we increase the event selection acceptance by $\sim 10\%$. To model the complicated correlations between kinematic variables used in the trigger selection described above, we use a novel technique that uses NN functions to parametrize trigger efficiencies as a function of kinematic observables [11, 12].

Utilizing the above strategies to increase acceptance, we select events containing opposite-sign [22], same-flavor lepton pairs with $m_{\ell\ell}$ in a window ([76, 106] GeV/ c^2) centered on the mass of the Z boson. Additionally, we require at least two jets [23], with transverse energy $E_T > 25$ GeV for the leading jet, and $E_T > 15$ GeV for all other jets. All jets are required to come from the central region of the detector, $|\eta| < 2.0$.

We define a pre-tag region (PT) before applying b -quark jet identification, consisting of events with a reconstructed Z boson and two or more jets passing the criteria described above. We observe 33975 events in

the PT region, and expect a total background yield of $34\,200 \pm 4\,800$ events, where the quoted uncertainty includes both systematic and statistical contributions. We expect 13.6 ± 1.1 ZH signal events in the PT region, for $m_H = 115$ GeV/ c^2 . The dominant process in the PT region is Z +light-flavor (LF) jets (u , d , s , and gluon jets), accounting for $\sim 85\%$ of the total background. Z +heavy-flavor (HF) (b and c) jets events, which contribute less than 10% of the background, are a small contribution in the PT region, but become relatively more significant in the signal regions. These processes are modeled using ALPGEN [24] to simulate the hard-scatter process, and PYTHIA [25] for the subsequent hadronization. The Z +jets processes are simulated at leading order and require a K -factor of 1.4 [26] for normalization to NLO cross sections. Other small backgrounds include diboson (ZZ , WZ , and WW) events and $t\bar{t}$ events, simulated entirely with PYTHIA normalized to NLO [27] and NNLO [28] predictions, respectively. Finally, other processes, such as QCD multijet production, can produce two selected leptons in the event. For muon events, this background is modeled using same-charge muon pairs from data. For electron events, we measure the rate of jets passing the electron NN using collision data to estimate the contribution from these processes. This background accounts for $\sim 3\%$ of the background in the PT region.

We utilize two different b -quark-identifying algorithms to search for jets consistent with the $H \rightarrow b\bar{b}$ decay. The secondary vertex algorithm (SV) [29] identifies jets consistent with the decay of a long-lived b hadron by searching for displaced vertices. The SV algorithm has both a tight and a loose operating point – the loose point has better b -jet identification efficiency but also has a higher rate of jets incorrectly identified as b jets. The jet probability (JP) algorithm [30] uses track impact parameters relative to the primary vertex to construct a likelihood for all jet tracks to have originated from the primary vertex. Both algorithms have imperfect rejection of c -quark jets, allowing some events containing them to contribute to the final signal regions.

We use the combination of the two highest- E_T jets to form potential Higgs boson candidates. We use a hierarchy of tag combinations to define three independent signal regions. We first search for events with two tight SV tags – defining the double-tag (DT) region, the most sensitive. A second signal region includes events with one loose SV tag and one JP tag (LJP), and the third contains events with just one tight SV tag (ST). These three regions are combined to search for ZH production. Table I shows the expected numbers of events for the signal and background processes, as well as the observed data.

In this analysis, we use a one-dimensional signal discriminant while maintaining the simultaneous separation of $t\bar{t}$ and Z +jets events from the ZH signal that was previously accomplished through a two-dimensional discriminant [9]. This method also further enhances signal

TABLE I: Expected background and observed data events for the three independent signal regions. Also shown is the expected number of ZH signal events, for a SM Higgs boson with $m_H = 115$ GeV/ c^2 . Quoted uncertainties include both systematic and statistical contributions.

Process	ST	LJP	DT
Z +LF, $Z + c\bar{c}$	683 ± 65	61 ± 9	7.6 ± 1.2
$Z + b\bar{b}$	287 ± 72	58 ± 15	42 ± 10
$t\bar{t}$	69 ± 7	29 ± 2	26 ± 3
Diboson	42 ± 3	9.5 ± 0.7	6.7 ± 0.6
Other	46 ± 12	3.4 ± 0.3	0.2 ± 0.1
Background	1127 ± 134	160 ± 23	82 ± 15
Data	1143	160	85
ZH (Predicted)	4.5 ± 0.4	1.8 ± 0.1	1.7 ± 0.1

discrimination by using two additional NNs in a multi-stage method, as described below.

We first train a NN signal discriminant, using several kinematic variables such as the dijet mass and \cancel{E}_T , to distinguish the signal-like (trained with ZH simulated events) and background-like (trained using a mixture of all background processes) events. Each data and simulated event is sent through the same signal discriminants, with a unique function optimized for 11 different Higgs mass hypotheses, defined in increments of 5 GeV/ c^2 between 100 and 150 GeV/ c^2 .

The multi-stage method defines three samples (I, II, III) where events can enter the final distributions used for limit setting. The first step involves separating $t\bar{t}$ and Z +jets events. This is done using a NN function trained to separate these specific processes. A cut on the output of this discriminant is chosen to define a $t\bar{t}$ -enhanced sample (Sample I). Events which fail this cut and fall into Samples II or III are passed through a second NN function trained to separate b jets from charm and light flavor jets [31]. A cut on the output of this flavor separator function defines a sample containing mainly $Z + c\bar{c}$ and Z +LF backgrounds (Sample II), and a region enriched in b jets (Sample III). This multi-stage approach produces final output distributions with three samples enriched in various background processes, as seen in Fig. 1, where we add (0, 1, 2) to the signal discriminant output score for each event when the event falls in Sample (I, II, III) as described above. By enhancing the signal discrimination in this way, we increase the sensitivity of the analysis by $\sim 10\%$ over the technique used in Ref. [9]. We use these distributions to set limits on the ZH production cross section times $H \rightarrow b\bar{b}$ branching ratio.

We evaluate several systematic uncertainties on the background and signal events. A large source of systematic uncertainty arises from the cross section values used in the normalization of events: 40%, 10%, 6%, and 5%, for Z +HF [32], $t\bar{t}$, diboson, and ZH simulated events, respectively. An uncertainty of (1, 2, 5)% is applied to the (ST, LJP, DT) ZH samples after measuring changes

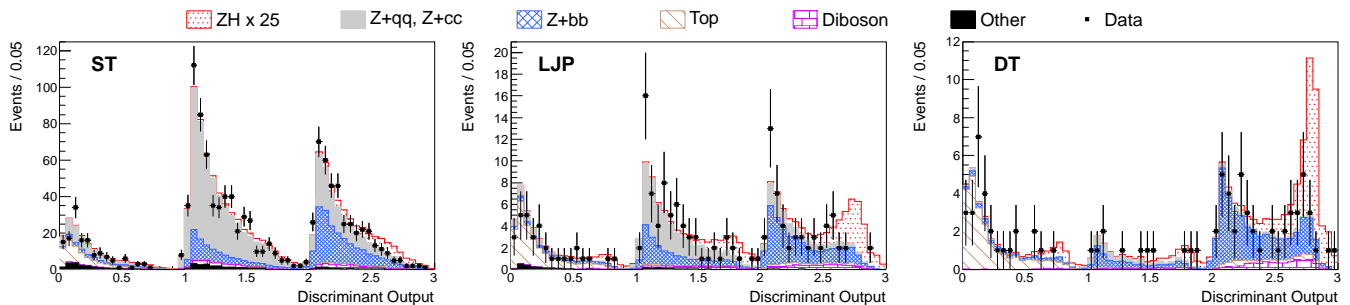


FIG. 1: Final discriminant output distributions for the three tag categories (ST, LJP, DT) used in this analysis. The distributions shown are for the discriminant trained on $m_H = 115 \text{ GeV}/c^2$ signal events. The ZH signal is shown, for $m_H = 115 \text{ GeV}/c^2$, and drawn scaled up by a factor of 25.

in acceptance using simulated events with more or fewer particles radiated by the incoming and outgoing partons. The mistag prediction is measured using data, and carries an uncertainty ranging from 13.5% (ST) to 28.8% (DT), depending on the tag category. To account for differing b -jet identification efficiencies in data and simulated events, uncertainties of 5.2% (ST), 8.7% (LJP), and 10.4% (DT) are applied to the b -tagged samples. A 6% uncertainty is applied to simulated events, accounting for uncertainty in the measurement of integrated luminosity. The trigger model applied to simulated events requires a 5% normalization uncertainty. We also apply uncertainties on the lepton reconstruction efficiency and energy measurement of 1% and 1.5%, respectively. For muons (electrons), we measure a 5% (50%) uncertainty on the normalization of the remaining background processes, based on differences in the rates of events containing same-charge and opposite-charge lepton pairs and in the rates of jets misidentified as electrons.

In addition, we account for sources of uncertainty that also include shape variations to account for the migration of events in the final signal discriminant distributions when fluctuating these shape-defining quantities within their uncertainties. These include uncertainties on the jet energies [33] as well as on the expected rate of $Z + \text{mistag}$ events.

Comparing the observed data to our background prediction including uncertainties, we do not find any evidence of a ZH signal. We set upper limits on the ZH production cross section times $H \rightarrow b\bar{b}$ branching ratio using a Bayesian algorithm [34], assuming a uniform prior on the signal rate. We do this by performing simulated experiments, each with a pseudo-dataset generated by randomly varying the normalizations of background processes within their respective statistical and systematic uncertainties, taking into account all background expectations in the absence of a signal. Each simulated experiment produces an upper limit on the ZH production cross section. The median of the 95% CL upper limits from the simulated experiments is taken to be the expected 95% CL upper limit of the analysis. We define the

TABLE II: Expected and observed 95% CL limits on the ZH production cross section times $H \rightarrow b\bar{b}$ branching ratio, relative to the expected standard model value, for each Higgs mass (in GeV/c^2) hypothesis.

m_H	100	105	110	115	120	125	130	135	140	145	150
Exp.	2.7	3.1	3.4	3.9	4.7	5.5	7.0	8.7	12	17	28
Obs.	2.8	3.3	4.4	4.8	5.4	4.9	6.6	7.3	10	14	22

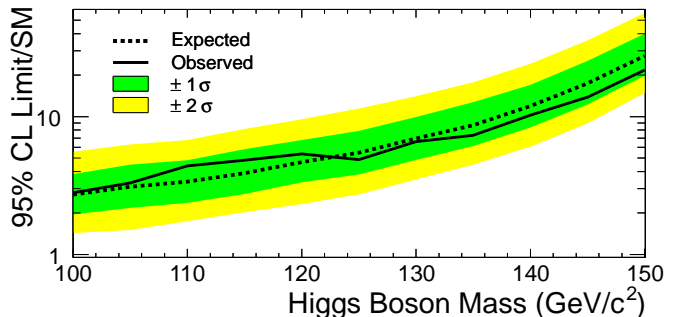


FIG. 2: Limits on the Higgs boson production cross section times the $H \rightarrow b\bar{b}$ branching ratio, given as a ratio to the standard model expected value.

1-sigma and 2-sigma deviations on the expected limit as the bounds which contain 68.3% and 95.5%, respectively, of the simulated experiment results. The observed data distribution is used to set the observed limit in a similar fashion. These limits are shown graphically, along with the 1-sigma and 2-sigma ranges, in Fig. 2. We find that the observed limit is in good agreement with the expected limit for no signal, within the 1-sigma range across all Higgs mass hypotheses.

In conclusion, we have performed a search for the standard model Higgs boson in the process $ZH \rightarrow \ell^+ \ell^- b\bar{b}$. The sensitivity of this analysis has improved due to several new multivariate techniques, including multivariate lepton identification, the use of NNs to obtain trigger efficiencies for simulated events, and a novel multi-stage discriminant approach used to enhance signal discrimina-

tion. We observe no significant excess and set an upper limit on the ZH production cross section times $H \rightarrow b\bar{b}$ branching ratio. We expect (observe) a limit of 3.9 (4.8) times the standard model predicted value, for a Higgs boson with mass $m_H = 115 \text{ GeV}/c^2$, at the 95% CL. The novel techniques presented here improve the sensitivity of the analysis by $\sim 25\%$ above the gain expected from the $\sim 85\%$ larger dataset.

We thank the Fermilab staff and the technical staffs of the participating institutions for their vital contributions. This work was supported by the U.S. Department of Energy and National Science Foundation; the Italian Istituto Nazionale di Fisica Nucleare; the Ministry of Education, Culture, Sports, Science and Technology of Japan; the Natural Sciences and Engineering Research Council of Canada; the National Science Council of the Republic of China; the Swiss National Science Foundation; the A.P. Sloan Foundation; the Bundesministerium für Bildung und Forschung, Germany; the Korean World Class University Program, the National Research Foundation of Korea; the Science and Technology Facilities Council and the Royal Society, UK; the Russian Foundation for Basic Research; the Ministerio de Ciencia e Innovación, and Programa Consolider-Ingenio 2010, Spain; the Slovak R&D Agency; the Academy of Finland; and the Australian Research Council (ARC).

-
- [1] P. W. Higgs, Phys. Rev. Lett. **13**, 508 (1964).
 [2] F. Englert and R. Brout, Phys. Rev. Lett. **13**, 321 (1964).
 [3] G. S. Guralnik, C. R. Hagen, and T. W. B. Kibble, Phys. Rev. Lett. **13**, 585 (1964).
 [4] R. Barate *et al.* (LEP Working Group), Phys. Lett. B **565**, 61 (2003).
 [5] The CDF and D0 Collaborations and the TEVNPH Working Group (2011), arXiv:1107.5518, FERMILAB-CONF-11-354-E.
 [6] G. Aad *et al.* (ATLAS Collaboration) (2012), CERN-PH-EP-2012-019, arXiv:1202.1408.
 [7] S. Chatrchyan *et al.* (CMS Collaboration) (2012), CERN-PH-EP-2012-023, arXiv:1202.1488.
 [8] A. Djouadi, J. Kalinowski, and M. Spira, Comput. Phys. Commun. **108**, 56 (1998).
 [9] T. Aaltonen *et al.* (CDF Collaboration), Phys. Rev. Lett. **105**, 251802 (2010).
 [10] V. M. Abazov *et al.* (D0 Collaboration), Phys. Rev. Lett. **105**, 251801 (2010).
 [11] S. Lockwitz, Ph.D. thesis, Yale University (2011), FERMILAB-THESIS-2012-02.
 [12] J. Pilot, Ph.D. thesis, The Ohio State University (2011), FERMILAB-THESIS-2011-42.
 [13] D. Acosta *et al.* (CDF Collaboration), Phys. Rev. D **71**, 052003 (2005).
 [14] We use a cylindrical coordinate system with z along the proton beam direction, r the perpendicular radius from the central axis of the detector, and ϕ the azimuthal angle. For θ the polar angle from the proton beam, we define $\eta = -\ln \tan(\theta/2)$, transverse momentum $p_T = p \sin \theta$ and transverse energy $E_T = E \sin \theta$.
 [15] A. Hocker *et al.*, PoS **ACAT**, 040 (2007).
 [16] L. Balka *et al.*, Nucl. Instrum. Methods **267**, 272 (1988).
 [17] M. Albrow *et al.*, Nucl. Instrum. Methods **480**, 524 (2002).
 [18] A. Abulencia *et al.* (CDF Collaboration), J. Phys. G **34**, 2457 (2007).
 [19] E. Thomson *et al.*, IEEE Trans. Nucl. Sci. **49**, 1063 (2002).
 [20] The missing transverse energy, $\vec{\cancel{E}}_T$, is defined by $\vec{\cancel{E}}_T = -\sum_i E_T^i \hat{n}^i$, where i is the number of the calorimeter tower with $|\eta| < 3.6$ and \hat{n}^i is a unit vector perpendicular to the beam axis and pointing at the i^{th} calorimeter tower. We also define $\cancel{E}_T = |\vec{\cancel{E}}_T|$.
 [21] A. Bhatti *et al.*, IEEE Trans. Nucl. Sci. **56**, 1685 (2009).
 [22] Forward ($|\eta| > 1.1$) electrons are exempt from this requirement, due to inaccurate charge determination.
 [23] G. C. Blazey and B. L. Flaugher, Annu. Rev. Nucl. Part. Sci. **49**, 633 (1999).
 [24] M. L. Mangano, M. Moretti, F. Piccinini, R. Pittau, and A. D. Polosa, J. High Energy Phys. **07**, 001 (2003).
 [25] T. Sjostrand, S. Mrenna, and P. Z. Skands, J. High Energy Phys. **05**, 026 (2006).
 [26] F. Febres Cordero, L. Reina, and D. Wackerroth, Phys. Rev. D **78**, 074014 (2008).
 [27] J. M. Campbell and R. Ellis, Phys. Rev. D **60**, 113006 (1999).
 [28] U. Langenfeld, S. Moch, and P. Uwer, Phys. Rev. D **80**, 054009 (2009).
 [29] D. Acosta *et al.* (CDF Collaboration), Phys. Rev. D **71**, 052003 (2005).
 [30] A. Abulencia *et al.* (CDF Collaboration), Phys. Rev. D **74**, 072006 (2006).
 [31] S. Richter, Ph.D. thesis, Karlsruhe Institute of Technology (2007), FERMILAB-THESIS-2007-35.
 [32] A. Abulencia *et al.* (CDF Collaboration), Phys. Rev. D **74**, 032008 (2006).
 [33] A. Bhatti *et al.*, Nucl. Instrum. Methods A **566**, 375 (2006).
 [34] K. Nakamura *et al.* (Particle Data Group), J. Phys. G **37** (2010).